requirements on the local operations. Following our scheme, error probabilities at the one per cent level can be achieved with present technology. In particular, the precision of linear optical elements such as PBS can be extremely high, with errors as low as one-tenth of one per cent or even less. Finally, we emphasize that there is an enormous difference in the experimental effort required between implementing the CNOT operation and overlapping two photons on a PBS. We believe that the present proposal might be a vital ingredient in the future realization of long-distance quantum communication. □

Received 27 November 2000; accepted 21 February 2001.

1. Bennett, C. H. & Brassard, G. in *Proc. IEEE Int. Conf. on Computers, Systems and Signal Processing* 175–179 (IEEE, New York, 1984).
2. Ekert, A. Quantum cryptography based on Bell's theorem. *Phys. Rev. Lett.* **67,** 661–663 (1991).
3. Bennett, C. H. *et al.* Teleporting an unknown quantum state via dual classical and Einstein-Podolsky-Rosen channels. *Phys. Rev. Lett.* **70,** 1895–1898 (1993).
4. Bennett, C. H. *et al.* Purification of noisy entanglement, and faithful teleportation via noisy channels. *Phys. Rev. Lett.* **76,** 722–725 (1996).
5. Deutsch, D. *et al.* Quantum privacy amplification and the security of quantum cryptography over noisy channels. *Phys. Rev. Lett.* **77,** 2818–2821 (1996).
6. Duan, L. M., Giedke, G., Cirac, J. L. & Zoller, P. Entanglement purification of gaussian continuous variable quantum states. *Phys. Rev. Lett.* **84,** 4002–4005 (2000).
7. Bose, S., Vedral, V. & Knight, P. L. Purification via entanglement swapping and conserved entanglement. *Phys. Rev. A* **60,** 194–197 (1999).
8. Briegel, H.-J., Duer, W., Cirac, J. I. & Zoller, P. Quantum repeaters: The role of imperfect local operations in quantum communication. *Phys. Rev. Lett.* **81,** 5932–5935 (1998).
9. Bennett, C. H. & DiVincenzo, D. P. Quantum information and computation. *Nature* **404,** 247–255 (2000).
10. Bennett, C. H. & Wiesner, S. J. Communication via one- and two-particle operators on Einstein-Podolsky-Rosen states. *Phys. Rev. Lett.* **69,** 2881–2884 (1992).
11. Mattle, K., Weinfurter, H., Kwiat, P. G. & Zeilinger, A. Dense coding in experimental quantum communication. *Phys. Rev. Lett.* **76,** 4656–4659 (1996).
12. Bouwmeester, D. *et al.* Experimental quantum teleportation. *Nature* **390,** 575–579 (1997).
13. Pan, J.-W., Bouwmeester, D., Weinfurter, H. & Zeilinger, A. Experimental entanglement swapping: Entangling photons that never interacted. *Phys. Rev. Lett.* **80,** 3891–3894 (1998).
14. Bouwmeester, D., Pan, J.-W., Weinfurter, H. & Zeilinger, A. High-fidelity teleportation of independent qubits. *J. Mod. Opt.* **47,** 279–289 (2000).
15. Jennewein, T., Simon, C., Weihs, G., Weinfurter, H. & Zeilinger, A. Quantum cryptography with entangled photons. *Phys. Rev. Lett.* **84,** 4729–4732 (2000).
16. Naik, D. S., Peterson, C. G., White, A. G., Berglund, A. J. & Kwiat, P. G. Entangled state quantum cryptography: eavesdropping on the Ekert protocol. *Phys. Rev. Lett.* **84,** 4733–4736 (2000).
17. Tittel, W., Brendel, T., Zbinden, H. & Gisin, N. Quantum cryptography using entangled photons in energy-time Bell states. *Phys. Rev. Lett.* **84,** 4737–4740 (2000).
18. Wootters, W. K. & Zurek, W. H. A single quantum cannot be cloned. *Nature* **299,** 802–803 (1982).
19. Monroe, C., Meekhof, D. M., King, B. E., Itano, W. M. & Wineland, D. J. Demonstration of a fundamental quantum logic gate. *Phys. Rev. Lett.* **75,** 4714–4717 (1995).
20. Rauschenbeutel, A. *et al.* Coherent operation of a tunable quantum phase gate in cavity QED. *Phys. Rev. Lett.* **83,** 5166–5169 (1999).
21. Knill, E., Laflamme, R. & Milburn, G. J. A scheme for efficient quantum computation with linear optics. *Nature* **409,** 46–52 (2001).
22. Bouwmeester, D., Pan, J.-W., Daniell, M., Weinfurter, H. & Zeilinger, A. Observation of three-photon Greenberger-Horne-Zeilinger entanglement. *Phys. Rev. Lett.* **82,** 1345–1349 (1999).
23. Pan, J.-W., Bouwmeester, D., Daniell, M., Weinfurter, H. & Zeilinger, A. Experimental test of quantum nonlocality in three-photon Greenberger-Horne-Zeilinger entanglement. *Nature* **403,** 515–519 (2000).
24. Takeuchi, S., Yamamoto, Y. & Hogue, H. H. Development of a high-quantum-efficiency single-photon counting system. *Appl. Phys. Lett.* **74,** 1064–1065 (1999).
25. Sanaka, K., Kawahara, K. & Kuga, T. New high-efficiency source of photon pairs for engineering quantum entanglement. Preprint quant-ph/0012028 at ⟨http://xxx.lanl.gov⟩ (2000).
26. Tanzilli, S. *et al.* Highly efficient photon-pair source using a periodically poled lithium niobate waveguide. Preprint quant-ph/0012053 at ⟨http://xxx.lanl.gov⟩ (2000).
27. Pan, J.-W. & Zeilinger, A. Greenberger-Horne-Zeilinger-state analyzer. *Phys. Rev. A* **57,** 2208–2211 (1998).
28. Bouwmeester, D. Bit-flip-error rejection in optical quantum communication. *Phys. Rev. A* **63,** R040301 (2001).
29. Yamamoto, T., Koashi, M. & Imoto, N. A concentration scheme for two partially entangled photon pairs. Preprint quant-ph/0101042 at ⟨http://xxx.lanl.gov⟩ (2001).
30. Cerf, N. J., Adami, C. & Kwiat, P. G. Optical simulation of quantum logic. *Phys. Rev. A* **57,** R1477–1480 (1998).

Acknowledgements

We thank L.-M. Duan, H. Ritsch, T. Tyc, L. Vaidman, P. Zoller and M. Zukowski for discussions. This work was supported by the Austrian Science Foundation FWF, the Austrian academy of sciences, and the TMR and QIPC programmes of the European Union.

Correspondence and requests for materials should be addressed to A.Z. (e-mail: Zeilinger-office@exp.univie.ac.at).

Mobile silver ions and glass formation in solid electrolytes

P. Boolchand & W. J. Bresser

Department of Electrical & Computer Engineering and Computer Science, University of Cincinnati, Cincinnati, Ohio 45221-0030, USA

Solid electrolytes are a class of materials in which the cationic or anionic constituents are not confined to specific lattice sites, but are essentially free to move throughout the structure. The solid electrolytes AgI and Ag_2Se (refs 1–7) are of interest for their use as additives in network glasses[8–12], such as chalcogenides and oxides, because the resulting composite glasses can show high electrical conductivities with potential applications for batteries, sensors and displays. Here we show that these composite glasses can exhibit two distinct types of molecular structures—an intrinsic phase-separation that results in a bimodal distribution of glass transition temperatures, and a microscopically homogeneous network displaying a single glass transition temperature. For the first case, the two transition temperatures correspond to the solid-electrolyte glass phase and the main glass phase (the 'base glass'), enabling us to show that the glass transition temperatures for the AgI and Ag_2Se phases are respectively 75 and 230 °C. Furthermore, we show that the magnitude of the bimodal glass transition temperatures can be quantitatively understood in terms of network connectivity, provided that the Ag^+ cations undergo fast-ion motion in the glasses. These results allow us to unambiguously distinguish base glasses in which these additives are homogeneously alloyed from those in which an intrinsic phase separation occurs, and to provide clues to understanding ion-transport behaviour in these superionic conductors.

The electrical conductivity of AgI becomes very high ($1\ \Omega^{-1}\ cm^{-1}$) at temperatures greater than 147 °C in the high-temperature phase (α-phase), when Ag^+ ions become mobile and contribute to fast-ion conduction[1]. In the companion iodide, $RbAg_4I_5$, fast-ion conduction occurs at room temperature[2], and the material has found applications as a solid electrolyte in portable batteries for heart pacemakers. The solid electrolytes AgI and Ag_2Se have also received widespread[3–7] attention as additives in network glasses, particularly chalcogenides and oxides, because of the unprecedented increase in conductivities of up to $10^{-1}\ \Omega^{-1}\ cm^{-1}$ with minuscule activation energies of 0.25 eV at room temperature. The microscopic origin of such behaviour has been the subject of continued investigations[3–7], although a consensus on the subject has yet to emerge. New insights into glass structure have recently emerged from compositional trends in glass transition temperature (T_g) that serve as a global measure of network connectivities[8]. Here we show that when the electrolytes Ag_2Se and AgI are added to chalcogenide base glasses, these electrolyte glasses in certain cases can display distinct glass transition temperatures (T_g). Constraint counting algorithms[9] reveal that the observed T_g values here provide a quantitative measure of network connectivity. The microscopic origin of glass formation is traced to Ag^+ acting as a fast diffuser, lowering the effective count of lagrangian bonding constraints[9] per atom (n_c), and promoting glass formation.

We have examined glass transitions in pseudobinary A_xB_{1-x} glasses—where A indicates additive (AgI or Ag_2Se) and B indicates chalcogenide base glass ($GeSe_4$ or As_2Se_3)—using temperature-modulated differential scanning calorimetry (MDSC). Syntheses of the glasses are described in Methods. Some of these glasses are found to be intrinsically phase-separated[10] (case I), and display bimodal T_g values—one ascribed to the base glass and the other to the additive solid-electrolyte glass phase. But some glass systems (case III) occur in which the additive and base materials

homogeneously alloy to display a single T_g, which is found to decrease progressively in proportion to the additive concentration. Last, some glass systems show an intermediate behaviour (case II), in which a part of the additive phase-separates while the remainder alloys with the base glass.

Figure 1, scan B, shows an MDSC scan of $GeSe_{3.54}$ base glass containing 18.2 mol% of AgI; scan C shows As_2Se_3 base glass containing 15.0 mol% of AgI. For comparison, we have also included a heating scan of β-AgI alone (scan A); this shows the onset of the endothermic β⟶α transition near 147 °C. In scans B and C, there is evidence for two glass transitions. The broad endothermic feature centred near T = 75 °C, common to both glass samples, is identified as the T_g of AgI glass. The transitions at higher temperatures are identified with the base glasses[11,12] in question. AgI in $GeSe_4$ base glass (scan B) thus appears to be a model example of a system that is nearly completely phase-separated (case I). On the other hand, AgI as an additive in As_2Se_3 base glass (scan C) appears to play a dual role (case II); part of it phase-separates (displaying the T_g = 75 °C), and the rest alloys with the base glass to lower the T_g of the latter from its pristine value[12] (shown by an arrow in scan C). Furthermore, the fraction of the endotherm at T_g = 75 °C is found to grow in proportion to the molar fraction of AgI in the glasses (see Supplementary Information), supporting the suggested T_g assignments.

In Fig. 2 we show MDSC results on two base glasses, each containing 10 mol% of Ag_2Se: $GeSe_4$ (scan B) and As_2Se_3 (scan C). We also show a heating scan on β-Ag_2Se alone, showing the β⟶α transition (onset) near 133 °C (scan A). In scan B, there are two distinct endothermic features (case I); a primary one at T_g = 180 °C due to $GeSe_4$ base glass[11], and a secondary one at T_g = 230 °C due to Ag_2Se glass[10]; the fraction of the latter endotherm increases in proportion to the Ag_2Se molar fraction (see Supplementary Information). On the other hand, Ag_2Se added to the As_2Se_3 base glass appears to alloy homogeneously (case III); neither the T_g of Ag_2Se glass nor that of As_2Se_3 base glass (arrow in scan C) are seen, but instead there is a significantly reduced T_g (scan C). This result is not unexpected, given that a melt of equimolar concentrations of Ag_2S and As_2S_3 (that is, $AgAsS_2$) upon cooling forms a solid that can exist[13] either as a stoichiometric crystal or as a bulk glass in which Ag and As are both 3-fold coordinated, leading to a network backbone that is optimally constrained (n_c = 3).

Counting algorithms based on lagrangian bonding constraints—including bond-stretching and bond-bending—have proved to be helpful[9] in understanding the glass-forming tendency in chalcogenide glasses. Furthermore, stochastic agglomeration theory[14,15] has provided the tool to correlate quantitatively the variation of T_g with network connectivity[8]. The mechanically effective connectivity of a network can be lowered when constraints are intrinsically broken[16]. For the case of SiO_2 glass, the bond-bending constraint of oxygen atoms is intrinsically broken[16] because the bridging bond angle (Si–O–Si) in the glass network is found to display wide excursions (100–180°). These ideas can be extended to the present solid electrolytes. The structure factor of liquid Ag_2Se has been modelled[17] after α-Ag_2Se, and can also serve as a good starting point to describe the structure of the bulk glass. The rapid diffusion of Ag^+ ions through the tetrahedral interstitial sites is due to a delicate balance[18] between ionic and covalent forces; this balance makes the free energy difference, $E_6 - E_4$, between Ag taking on a coordination number of 6 (E_6) and of 4 (E_4) to nearly vanish. α-AgI possesses a fractional ionicity of 0.77 on the Phillips[18] scale, close to the threshold value of 0.785 when $E_6 = E_4$. If the I–Ag–I bond-angle flexes as Ag moves, then we expect the Ag–I–Ag bond-angle also to flex, leading to the general recognition that the bond-bending constraint about both cations (Ag^+) and anions (I^-, Se^{2-}) must be intrinsically broken in these solid electrolytes.

The structure of the superionic (α) phase of Ag_2Se and AgI is shown in Fig. 3. It consists of anions (Se, I) forming a body-centred cubic (b.c.c.) arrangement (shown blue) across which the Ag^+ cations rapidly diffuse, largely through the distorted tetrahedral interstitial sites[19] (shown red). In the case of α-Ag_2Se, on stoichiometric grounds, we must associate on average 4 Ag atoms and 2 Se atoms with the unit cell (Fig. 3), thus requiring 8 tetrahedral interstitial sites (red atoms) to be populated by Ag on the cube faces, as these are shared by two adjacent cubes. This leads to a coordination number of 4 and 8 for Ag and Se in α-Ag_2Se. For an atom possessing a coordination number, r, in a three-dimensional network, the number of independent bond-stretching constraints, n_{bs}, is given by $r/2$, while the number of bond-bending constraints, n_{bb}, is given by $2r - 3$. This gives the total number of constraints per

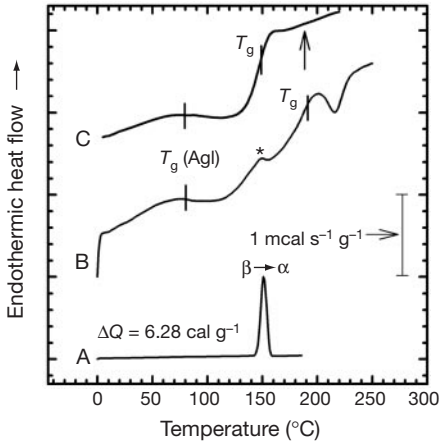

Figure 1 MDSC scans of AgI-based systems. A, the endothermic β⟶α transformation in β-AgI; B, two glass transitions in $Ge_{0.22}Se_{0.78}$ base glass containing 18.2 mol% AgI; C, two glass transitions in As_2Se_3 base glass containing 15 mol% AgI. In scans B and C, the broad feature with a T_g = 75 °C was due to AgI glass, while the second T_g at higher T was due to the base glasses. For the glass sample in scan B, a trace of β-AgI was quenched in, and shows evidence of the β⟶α transition, as indicated by the asterisk. Powder X-ray diffraction of the sample confirmed the presence of β-AgI traces. In scan C, the T_g of the base glass is shifted down by 25 °C from the T_g of pristine As_2Se_3 shown by an arrow.

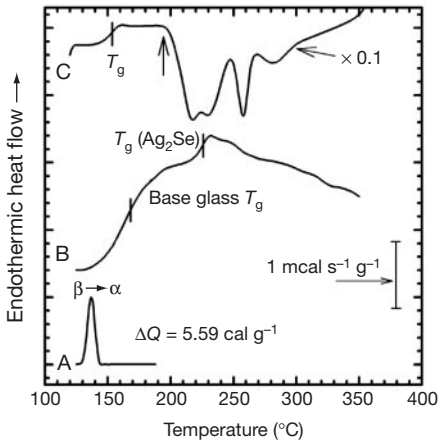

Figure 2 MDSC scans of Ag_2Se-based systems. A, β-Ag_2Se showing the β⟶α transition onset at 133 °C; B, $GeSe_4$ base glass containing 10 mol% Ag_2Se, showing two T_g values, one at 180 °C (ascribed to the base glass) and the other at 230 °C (ascribed to Ag_2Se glass); C, As_2Se_3 base glass containing 10 mol% Ag_2Se, showing one T_g at 160 °C ascribed to a homogeneously alloyed glass. In scan C, the reduction of the observed T_g from that in pristine As_2Se_3 (shown by arrow) is the result of the additive mixing with the base network to lower the global connectivity of the alloyed network.

atom, $\bar{n}_c$, as $(5/2)\bar{r} - 3$. Enumeration of bond-stretching constraints $(r/2)$ for both Se^{2-} anions and Ag^+ cations then gives the total number of constraints for the 6 atoms in the b.c.c. cell of:

$$2[n_{bs}(Se)] + 4[n_{bs}(Ag)] = 2[4] + 4[2] = 16 \quad (1)$$

This yields $6\bar{n}_c = 16$ or $\bar{n}_c = 2.66$. The mechanically effective connectivity $(\bar{r}_m)$ of such a network is then related to $\bar{n}_c$ as follows:

$$\bar{n}_c = 5/2\bar{r}_m - 3 \quad \text{or} \quad \bar{r}_m(Ag_2Se) = 2.26 \quad (2)$$

In the case of α-AgI, on stoichiometric grounds, we must associate 2 Ag atoms with the 2 I atoms in the unit cell (Fig. 3), thus requiring 4 tetrahedral interstitial sites to be occupied by Ag. This leads to a coordination number of 4 for both Ag and I atoms. Enumeration of bond-stretching constraints for both Ag^+ and I^- gives the total number of constraints for the 4 atoms in the body-centred cubic (b.c.c.) cell:

$$2[n_{bs}(I)] + 2[n_{bs}(Ag)] = 2[2] + 2[2] = 8 \quad (3)$$

This yields $4\bar{n}_c = 8$ or $\bar{n}_c = 2$. For $\bar{n}_c = 2$, equation (2) shows the mechanically effective coordination of AgI glass to be $\bar{r}_m = 2$, suggesting that the morphological structure of the glass may be similar to that of Se glass.

In the binary chalcogenide glasses (Si-Se, Ge-Se), a linear increase of T_g values with $\bar{r}_m$ (Fig. 4) at low $\bar{r}$ (< 2.20) has been found[8]. This has been analysed[14,15] in terms of a random cross-linking of Se_n-chains by the tetrahedrally coordinated (coordination number 4) group IV (Si, Ge) atoms. The stochastic agglomeration theory[14,15] predicts a parameter-free slope, $dT_g/d\bar{r}_m$, that is in excellent accord with measured[8] T_g changes. On this plot (Fig. 4), we have also shown the observed T_g values of AgI and Ag_2Se, and find the suggestion of a sharper increase of T_g with $\bar{r}_m$ (broken curve in Fig. 4) in the present solid-electrolyte glasses. We expect the $T_g(\bar{r}_m)$ variation to exhibit a power-law behaviour, as the coordination number of the anions (I^-, Se^{2-}) increases progressively from 4 to 8 in going from AgI to Ag_2Se. (Such behaviour would be in sharp contrast to the case of the binary chalcogenides, in which increases in global connectivity are brought about by increasing the content of group IV atoms possessing a fixed coordination number of 4.) This idea could be tested by examining $T_g(z)$ variation in $(AgI)_{1-z}(Ag_2Se)_z$ alloy glasses connecting the two end-member compositions ($z = 0,1$), and analysing the results using stochastic agglomeration theory: we are at present doing this. If Ag were not a fast diffuser in the electrolyte melts, the mechanically effective coordination numbers of Ag_2Se and AgI would be rather high and would preclude[9] glass formation. Thus, constraint-counting algorithms reveal the connection between glass-forming tendency and fast-ion conduction in these archetypal solid electrolytes.

When AgI and Ag_2Se are added to chalcogenide base glasses, they form glasses largely when the base glass is optimally constrained ($\bar{n}_c = 3$). Thus, these additives will spontaneously crystallize to β-AgI and β-Ag_2Se in an underconstrained Se base glass ($\bar{n}_c = 2$) or in an overconstrained $Ge_{0.30}Se_{0.70}$ base glass ($\bar{n}_c = 3.50$), but these electrolytes will form glasses in an optimally constrained ($\bar{n}_c = 3$) base glass such as $GeSe_4$ and As_2Se_3. This is perhaps due to the absence of connectivity-induced mechanical stress when the backbone is optimally constrained[12]. Near $\bar{n}_c = 3$, the base network is known to self-organize[20] and become stress-free[12], making it easy for the additive to finely disperse and form a bulk glass, whose signature constitutes the observation of a T_g.

The chemical alloying behaviour of the solid-electrolyte additives in the present chalcogenides may have close parallels to their behaviour in oxide glasses[3,4,6,7,21,22]. In those instances (case I) where AgI glass completely phase-separates from the base glass, we expect conductivity to display a threshold behaviour corresponding to the volume percolation transition[23] of the electrolyte phase for which there may already be electrical transport evidence[4,24]—although this needs to be confirmed structurally. On the other extreme (case III), alloys composed of a 2:1 molar ratio of AgI to Ag_2SeO_4, in which the equal-sized $(SeO_4)^{2-}$ and I^- anions can intimately mix (chemical disorder) to promote glass formation, show[21,22] a Se-glass-like T_g = 50 °C characteristic of an undercoordinated $r_m = 2$ network, again in harmony with the present counting of lagrangian constraints. And the enhancement of electrical conductivity in such homogeneously alloyed systems may be due to a reduced activation energy upon an increase in

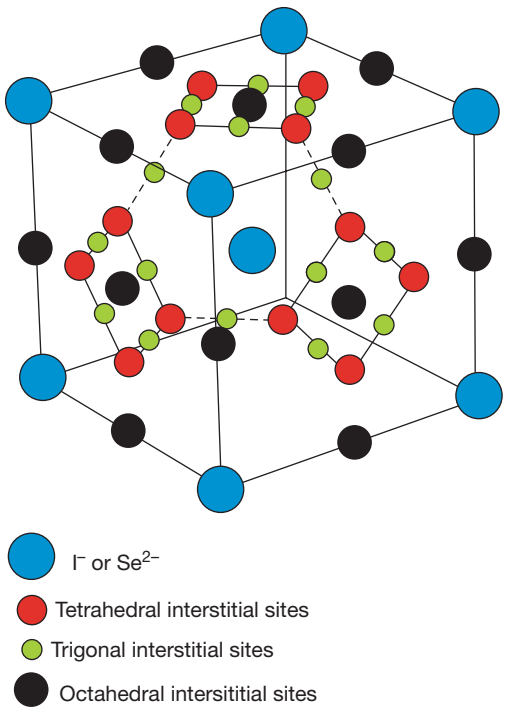

Figure 3 The crystal structure of α-Ag_2Se and α-AgI. The Se^{2-} and I^- anions (shown blue) form a b.c.c. unit, with the Ag cations rapidly diffusing across distorted tetrahedral interstitial sites (shown red) through the trigonal interstitial sites (shown green). The black circles show distorted octahedral sites.

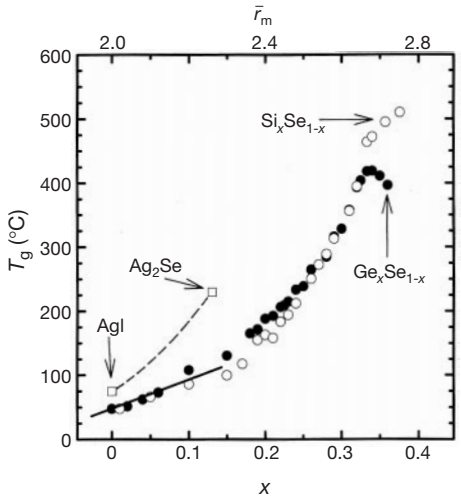

Figure 4 Variations of the glass transition temperature (T_g) of binary Ge_xSe_{1-x} and Si_xSe_{1-x} glasses. The data are taken from ref. 8, and reveal a regime ($2 < \bar{r}_m < 2.2$) of linear variation. The straight line represents the prediction of stochastic agglomeration theory[14,15]. On the other hand, T_g values in the present electrolytes may form part of a nonlinear variation sketched by the dashed line. See text for details.

molar volumes[25] of the base network upon AgI addition; such increases in molar volumes also progressively lower the T_g of the alloyed glasses (Fig. 1c, Fig. 2c).

Determining the physics of transport in ionic glasses continues to be challenging. It is necessary to understand aspects of molecular structure in order to understand the details[24,26] of the conduction process. In this respect, the identification of the glass transition temperatures of AgI and Ag_2Se will also be helpful in understanding the phase separation of these additives in oxide glasses. □

Methods

Stoichiometric As_2Se_3, AgI and elemental Ge, Ag and Se (99.999% purity from Cerac, Inc.) were used as starting materials to synthesize the pseudobinary A_xB_{1-x} alloy glasses (see text). Details of glass synthesis are in our earlier[10] work, where we examined the role of Ag as an additive in Ge-Se base glasses. T_gs were measured using a model 2920 MDSC (T.A. Instruments, Inc.) at a scan rate of 3 °C min^{-1}, and modulation rate of 1 °C per 100 s.

Received 16 November 2000; accepted 20 February 2001.

1. Tubandt, C. & Lorenz, E. Molekularzustand und elektrisches Leitvermögen kristallisierter Salze. *Z. Phys. Chem.* **24,** 513–543 (1914).
2. Bradley, J. N. & Greene, P. D. Solids with high ionic conductivity in group I halide system. *Trans. Faraday Soc.* **63,** 424–430 (1967).
3. Minami, T., Imazawa, K. & Tanaka, M. Formation region and characterization of superionic conductivity glasses in the systems AgI-Ag_2O-M_xO_7. *J. Non-Cryst. Solids* **42,** 469–476 (1980).
4. Rousselot, C. *et al.* The origins of neutron scattering prepeaks and conductivity enhancement in AgI-containing glasses. *Solid State Ionics* **78,** 211–221 (1995).
5. Kincs, J. & Martin, S. W. Non-Arrhenius conductivity in glasses: mobility and conductivity saturation effects. *Phys. Rev. Lett.* **76,** 70–73 (1996).
6. Swenson, J., McGreevy, R. L., Börjesson, L., Wicks, J. D. & Howells, W. S. Intermediate-range structure of fast-ion-conductivity. *J. Phys. Condens. Matter* **8,** 3545–3552 (1996).
7. Angell, C. A. Mobile ions in amorphous solids. *Annu. Rev. Phys. Chem.* **43,** 693–717 (1992).
8. Boolchand, P. & Bresser, W. J. The structural origin of broken chemical order in $GeSe_2$ glass. *Phil. Mag. B* **80,** 1757–1772 (2000).
9. Phillips, J. C. Topology of covalent non-crystalline solids I: short range order in chalcogenide alloys. *J. Non-Cryst. Solids* **34,** 153–181 (1979).
10. Mitkova, M., Wang, Y. & Boolchand, P. Dual chemical role of Ag as an additive in chalcogenide glasses. *Phys. Rev. Lett.* **83,** 3848–3851 (1999).
11. Feng, X., Bresser, W. J. & Boolchand, P. Direct evidence for stiffness threshold in chalcogenide glasses. *Phys. Rev. Lett.* **78,** 4422–4425 (1997).
12. Georgiev, D. G., Boolchand, P. & Micoulaut, M. Rigidity transitions and molecular structure of As_xSe_{1-x} glasses. *Phys. Rev.* B **62,** R9228–R9232 (2000).
13. Slivka, V. Y., Vysochanskii, Y. M., Stefanovich, V. A., Gerasimenko, V. S. & Chepur, D. V. Features of the vibrational spectra of $AgAsS_2$. *Sov. Phys. Solid State* **24,** 392–398 (1982).
14. Kerner, R. & Micoulaut, M. On the glass transition temperature in covalent glasses. *J. Non-Cryst. Solids* **210,** 298–305 (1997).
15. Micoulaut, M. The slope equations: a universal relationship between local structure and glass transition temperature. *Eur. Phys. J. B* **1,** 277–294 (1998).
16. Zhang, M. & Boolchand, P. The central role of broken bond-bending constraints in promoting glass formation in the oxides. *Science* **266,** 1355–1357 (1994).
17. Barnes, A. C., Lague, B. S., Salmon, S. P. & Fischer, H. E. A determination of the structure of liquid Ag_2Se using neutron diffraction and isotopic substitution. *J. Phys. Condens. Matter.* **9,** 6159–6173 (1997).
18. Phillips, J. C. *Bonds and Bands in Semiconductors* 45 (Academic, New York, 1973).
19. Nield, V. M., Keen, D. A., Hayes, W. & McGreevy, R. L. Structure and fast-ion conduction in α-AgI. *Solid State Ionics* **66,** 247–258 (1993).
20. Thorpe, M. F., Jacobs, D. J., Chubynsky, M. V. & Phillips, J. C. Self-organization in network glasses. *J. Non-Cryst. Solids* **266–269,** 859–866 (2000).
21. Cramer, C., Price, D. L. & Saboungi, M. L. Structure of AgI/Ag_2SeO_4 fast-ion conducting glasses: neutron diffraction experiments. *J. Phys. Condens. Matter.* **10,** 6229–6242 (1998).
22. Shastry, M. C. R. & Rao, K. J. Physico-chemical investigation of fast ion conducting AgI-Ag_2SeO_4 glasses. *Proc. Ind. Acad. Sci.* **102,** 541–553 (1990).
23. Zallen, R. *The Physics of Amorphous Solids* 190 (Wiley & Sons, New York, 1998).
24. Bunde, A., Funke, K. & Ingram, M. D. Ionic glasses: History and challenges. *Solid State Ionics* **105,** 1–13 (1998).
25. Swenson, J. & Börjesson, L. Correlation between free volume and ionic conductivity in fast ion conducting glasses. *Phys. Rev. Lett* **7,** 3569–3572 (1996).
26. Roling, B., Happe, A., Funke, K. & Ingram, M. D. Carrier concentrations and relaxation spectroscopy: new information from scaling properties of conductivity spectra in ionically conducting glasses. *Phys. Rev. Lett.* **78,** 2160–2163 (1997).

Supplementary information is available on *Nature*'s World-Wide Web site (http://www.nature.com) or as paper copy from the London editorial office of *Nature*.

Acknowledgements

We thank D.H. McDaniel, M. Mitkova, D. Georgiev, B. Goodman and M. Micoulaut for discussions. This work was supported by the Solid State Physics Program of the National Science Foundation.

Correspondence and requests for materials should be addressed to P.B. (e-mail: punit.boolchand@uc.edu).

Absence of deep-water formation in the Labrador Sea during the last interglacial period

C. Hillaire-Marcel*, A. de Vernal*, G. Bilodeau* & A. J. Weaver†

** GEOTOP, Université du Québec à Montréal, CP 8888, Montreal, Quebec, H3C 3P8 Canada*

† School of Earth and Ocean Sciences, University of Victoria, PO Box 3055, British Colombia, V8W 3P6, Canada

The two main constituent water masses of the deep North Atlantic Ocean—North Atlantic Deep Water at the bottom and Labrador Sea Water at an intermediate level—are currently formed in the Nordic seas and the Labrador Sea, respectively[1]. The rate of formation of these two water masses tightly governs the strength of the global ocean circulation and the associated heat transport across the North Atlantic Ocean[2]. Numerical simulations have suggested a possible shut-down of Labrador Sea Water formation as a consequence of global warming[3]. Here we use micropalaeontological data and stable isotope measurements in both planktonic and benthic foraminifera from deep Labrador Sea cores to investigate the density structure of the water column during the last interglacial period, which was thought to be about 2 °C

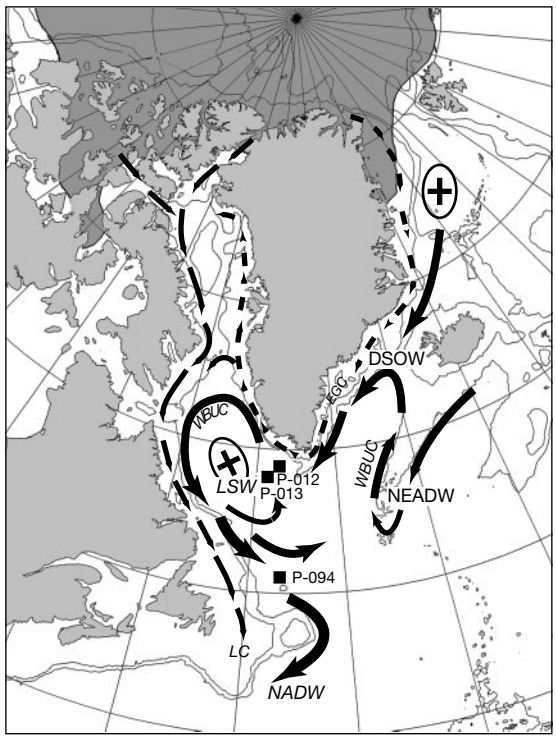

Figure 1 The Arctic–North Atlantic sector and the location of the study cores. Crosses: zones of formation of deep (DSOW) or intermediate (LSW) water. DSOW, Denmark Strait Overflow Water; LSW, Labrador Sea Water; NEADW, Northeast Atlantic Deep Water; NADW, North Atlantic Deep Water. Thin arrows, surface currents from the Fram Strait (dashed) and from the Arctic archipelago (continuous). EGC, East Greenland Current; LC, Labrador Current. Thick arrows, deep currents; WBUC, Western Boundary Undercurrent. The Arctic ice-pack (more than 11 months per year of sea-ice) is shown in dark grey. Coring sites were on the Greenland slope (P-012; 58° 55.35′ N, 47° 07.01′ W; 2,830 m), the Greenland rise (P-013; 58° 12.59′ N; 48° 22.40′ W; 3,380 m), and near Orphan knoll (P-094; 50° 12.26′ N, 45° 41.14′ W; 3,448 m).